Introduction to Wave-Particle Interactions and their Impact on Energetic Particles in Geospace

Kazue Takahashi and Yoshizumi Miyoshi

| 2.1 Introduction | 36 |
|--|------|
| 2.2 Impact of wave-particle interaction on electron | |
| acceleration and loss | 36 |
| 2.3 General observational approach to wave-particle interactions | s 38 |
| 2.4 Experimental resources | 39 |
| 2.5 Example of observational studies of waves and particles | 42 |
| 2.6 Summary | 46 |
| Acknowledgments | 47 |
| References | 47 |

■ Abstract

The magnetosphere is a natural plasma laboratory that contains a wide variety of waves excited by both disturbances in the solar wind and instabilities within the magnetosphere. The waves interact with particles in the outer zone radiation belt and ring current, thereby playing a fundamental role in redistributing the particles in spatial coordinates and energy as geomagnetic activity changes. We illustrate how observations from spacecraft and ground-based experiments can be used to advance our knowledge on the behavior of the particles. Examples include previous spacecraft observations of particle interactions with ultra-low-frequency waves, previous ground-based observations of electron precipitation caused by electromagnetic ion cyclotron (EMIC) waves, and planned satellite observations of nonlinear EMIC and whistler wave-particle interactions.

2.1 Introduction

The dynamic evolution of the ring current and radiation belts during geomagnetic storms is an important phenomenon not only as a target for scientific research but also as a practical matter of concern (space weather effects) for human activity both on the ground and in space. Essential to understanding and hopefully to predicting how the ring current and the radiation belts behave is observational determination of local wave-particle interactions and their global consequences. There are other processes that can change the particle distribution, for example, global reconfiguration of the magnetic field by large-scale structures in the solar wind. However, there is no question that wave-particle interactions make a critical contribution to particle acceleration and transport at times of high geomagnetic activity.

The geospace is a natural laboratory in which we can conduct in situ measurements of wave-particle interactions covering a wide range of wave frequencies, wavelengths, and particle energies. However, unlike in laboratories on the ground, we cannot control the boundary conditions or measurement locations in the magnetosphere to determine the causal relationship between various phenomena. Fortunately, modern spacecraft missions, some consisting of multiple probes, allow us to gain new information on waves and particles in the inner magnetosphere that could not be obtained a decade ago. For example, the Van Allen Probes mission consists of two probes that can separate spatial and temporal variations of the phase space density of energetic electrons. This, combined with ground-based remote sensing techniques and numerical simulations, provides us with opportunities to advance our knowledge about wave-particle interactions.

The objective of this chapter is to briefly review some of the wave-particle interactions that are believed to impact the outer radiation belt (3 < L < 7) during storms and how these processes can be studied using observational tools that are available now. For comprehensive overviews of the radiation belts, geomagnetic storms, and wave-particle interactions, readers are referred to recent articles (e.g., Hudson et al. 2008, Shprits et al. 2008a, 2008b, Thorne 2010, Ukhorskiy and Sitnov 2012, Miyoshi et al. 2012) as well as to other chapters in this book.

2.2 Impact of wave-particle interaction on electron acceleration and loss

Figure 2.1 is a summary diagram showing processes discussed much in the literature that lead to acceleration and transport of electrons in the inner magnetosphere. In this figure, the horizontal and vertical axes indicate distance from the Earth and electron kinetic energy, respectively. The effects of plasma waves on electrons are as follows. Interaction of electrons with Pc5 ultra-low-frequency (ULF) waves (1–10 mHz) ex-

cited by external source mechanisms conserves the first adiabatic invariant (magnetic moment) of the electrons but violates the third adiabatic invariant. As a consequence, plasmasheet electrons (L > 7, ~keV energy) are transported through the radial diffusion process (Fälthammar 1965, Schulz and Lanzerotti 1974) to the radiation belt (L < 7), where the energy can reach ~MeV. Here the energy exchange between electrons and waves occurs through the drift resonance, $\omega - m\omega_{\rm d} = 0$ (if an axisymmetric magnet field is assumed), where ω is the wave frequency, m is the azimuthal wave number, and $\omega_{\rm d}$ is the bounce averaged drift frequency (e.g., Elkington et al. 1999). Magnetosonic waves, excited between $f_{\rm cH^+}$ and $f_{\rm LH}$ (typically in the 1–10 Hz band) (Russell et al. 1970) possibly by proton ring distributions (Meredith et al. 2008), can locally accelerate electrons through the Landau resonance $\omega - k_{\parallel}v_{\parallel} = 0$ (Horne et al. 2007) or transit-time scattering (Bortnik and Thorne 2010), where $f_{\rm cH^+}$ is the

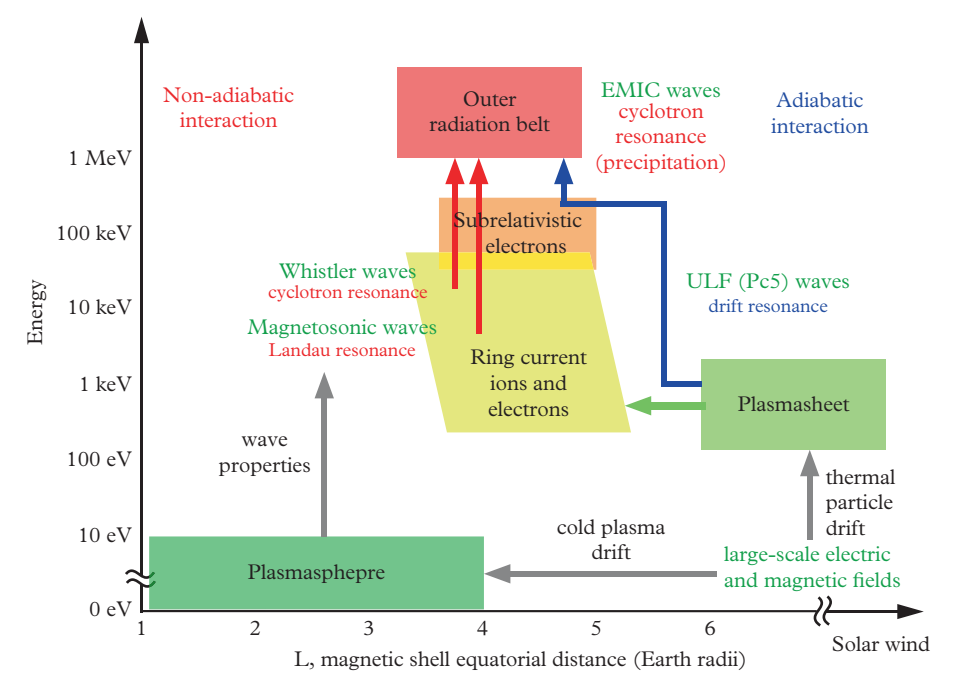


Figure 2.1 Diagram illustrating the relationship between magnetospheric regions, near-dc and wave fields, and acceleration and transport of electrons (slightly modified from Figure 2 of Miyoshi et al. (2012)). Domains in L and particle energy are shown by boxes, electromagnetic fields including waves are shown in green fonts, the processes that regulate the plasma domain and wave properties are shown by gray arrows, and electron acceleration/transport is shown by blue (adiabatic process) and red (non-adiabatic process) arrows.

proton gyro frequency, $f_{\rm LH}$ is the lower hybrid resonance frequency, and k_{\parallel} and v_{\parallel} are the wavenumber and particle velocity parallel to the magnetic field, respectively. Whistler mode chorus waves (Tsurutani and Smith, 1974), excited in two bands, ~ 0.1 –0.5 $f_{\rm ce}$ and ~ 0.5 –0.7 $f_{\rm ce}$, by hot (10–100 keV) ring-current energy electrons, can locally accelerate the electrons to \sim MeV via the electron cyclotron resonance $\omega - k_{\parallel}v_{\parallel} = 2\pi f_{\rm ce}/\gamma$ (e.g., Summers et al. 2002), where $f_{\rm ce}$ is the electron cyclotron frequency and γ is the relativistic factor. Electromagnetic ion cyclotron (EMIC) waves, excited below $f_{\rm cH^+}$, can also be in cyclotron resonance with electrons, which leads to pitch angle scattering of \sim MeV electrons into the atmospheric loss cone (Thorne and Kennel, 1971).

The main point of Figure 2.1 is that the wave phenomena are interconnected with the solar wind driving and internal kinetic and fluid processes. For example, high solar wind velocity enhances the Kelvin-Helmholtz instability on the magnetopause and generates ULF waves in the Pc5 band (e.g., Claudepierre et al. 2008). At the same time, the high solar wind velocity, combined with the southward component of the interplanetary magnetic filed, strengthens magnetospheric convection, causes the plasmasphere to shrink (e.g., Li et al. 2006), and enhances transport of plasmasheet particles to the inner magnetosphere though substorm injections (e.g., Miyoshi et al. 2013). Meanwhile, the inner magnetosphere, energetically pumped up by this solar wind action, will experience various plasma instabilities that excite waves spanning ULF (e.g., Ozeke and Mann 2001) to very-low-frequency (VLF) (e.g., Meredith et al. 2002) bands. Finally, configurational changes of the magnetosphere alter particle drift orbits and lead to particle loss through the magnetopause (Turner et al. 2013). Wave-particle interaction is also involved in the process of radiation belt electron loss. For example, ULF waves can diffuse the electrons radially outward if there is a peak phase space density within the radiation belt, and both EMIC waves (Thorne and Kennel 1971, Ukhorskiy et al. 2010) and whistler waves can scatter electrons into the loss cone (Kennel and Petschek 1966).

2.3 General observational approach to wave-particle interactions

Vastly different behaviors of the radiation belt have been reported for storms with similar histories of ring current evolution (e.g., Reeves et al. 2003). This finding could be understood only if we could keep track of each of the processes such as those illustrated in Figure 2.1 and then find their relative importance.

To tackle the above radiation belt mystery, the following approaches can be taken. (a) Determine the wave properties (frequency, amplitude, wave vector, and polarization) with in situ measurements. (b) Determine the local response (both linear and nonlinear) of particles to the waves with in situ measurements. (c) Evaluate the global consequence of the spatiotemporal variation of wave fields and particle fluxes with multipoint observations of selected events or with statistical analyses of data from a

small number of experimental resources. (d) Determine the connection of the solar wind input to the radiation belt dynamics to be able to predict the radiation belt behavior.

2.4 Experimental resources

Orbital properties of spacecraft dictate what we can achieve by in situ observations. Spacecraft with low-inclination orbits are best suited for exploring the radiation belt and ring current, because particles with all mirror latitudes pass the magnetic equator and the equator is the site where many wave modes are excited. Figure 2.2 shows orbits of

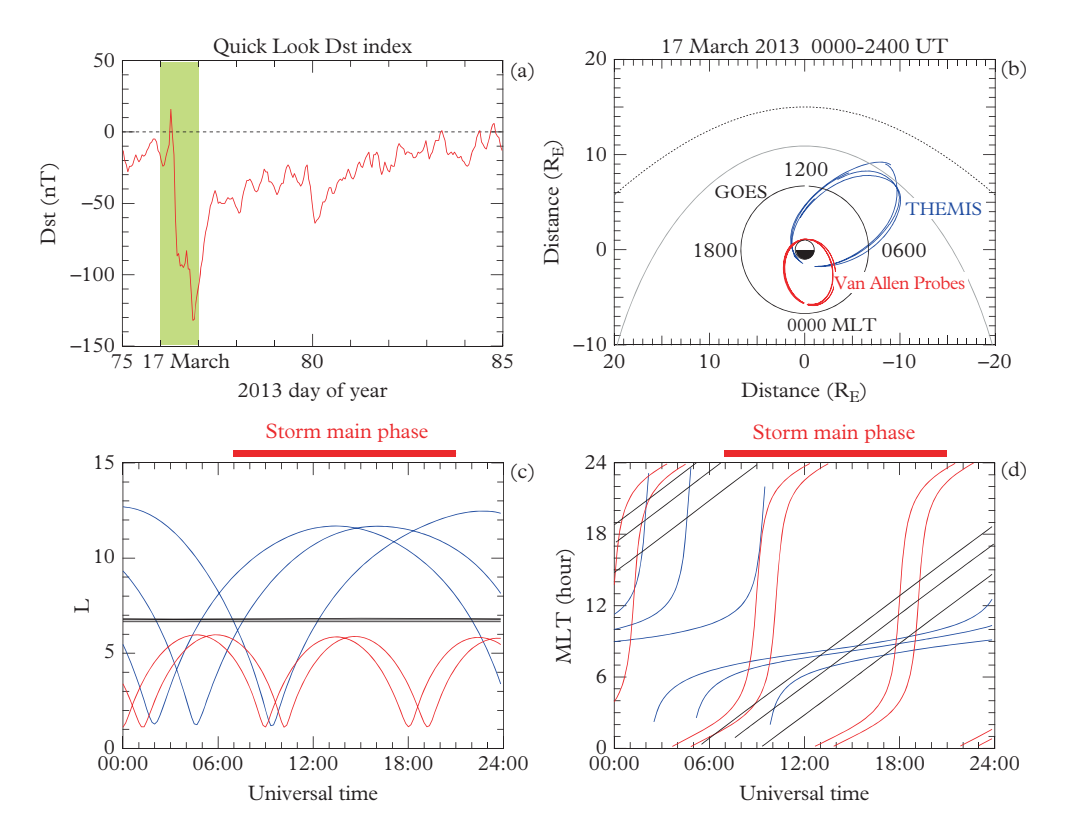


Figure 2.2 Position of Van Allen Probe-A and -B, THEMIS-A, -D, and -E, and GOES-13, -14, and -15 for a 24-hour period during a geomagnetic storm in March 2013. (a) Quick look Dst index (source: World Data Center for Geomagnetism, Kyoto). The shading indicates the period for which the satellite orbits are plotted. (b) L (radius) versus magnetic local time (MLT, azimuth) plots of the spacecraft orbits. The magnetic coordinates are defined using a dipole magnetic field. (c) Time series plots of L of the spacecraft. (d) Time series plots of MLT of the spacecraft.

such spacecraft including the two Van Allen Probes (orbital period \sim 9 hours, inclination \sim 10°) (Mauk et al. 2013), the three near-Earth THEMIS probes (orbital period \sim 24 hours, inclination 5–12°) (Angelopoulos 2008, Frey et al. 2008), and three GOES geostationary spacecraft (Singer et al. 1996). Orbits are shown for a 24-hour period encompassing the main phase of a geomagnetic storm (Figure 2.2a). The equatorial projection of the orbits (Figure 2.2b) indicates that the Van Allen Probes were in good position to observe substorm activity near midnight, while the THEMIS probes were positioned to detect direct influence of the solar wind as well as chorus emission expected on the dayside. Most importantly, the short orbital periods of the Van Allen Probes allow us to obtain several radial cuts of the radiation belts during the storm main phase (Figure 2.2c). The local time separation also varies (Figure 2.2d), so it is possible to study the azimuthal propagation velocity or wavelength of waves when two spacecraft are on the same L shell. The spacecraft separation can be much smaller than 1 $R_{\rm E}$, making it possible to determine wavelengths comparable to the Larmor radius (\sim 100 km) of ring current ions.

Comprehensive instrumentation is required on spacecraft to capture the different wave-particle interactions illustrated in Figure 2.1. If we take the Van Allen Probes as an example (Figure 2.3), the experiments on each spacecraft include a fluxgate magnetometer (to detect magnetohydynamic (MHD) and EMIC waves), a search coil magnetometer (whistler waves), an electric field detector (MHD, EMIC, and whistler waves), a plasma wave analyzer (plasma waves up to the upper hybrid band), a plasma analyzer (plasmasphere and plasmasheet), and energetic particle detectors (ring current and radiation belts) (Wygant et al. 2013, Kletzing et al. 2013, Funsten et al. 2013, Baker et al. 2013, Blake et al. 2013, Mitchell et al. 2013, Mazur et al. 2013). The major ions, H⁺, He⁺, and O⁺, are distinguished because they behave differently during geomagnetic storms (Hamilton et al. 1988). Electron number density is routinely determined from the spacecraft potential or from the spectral features in plasma wave spectra, usually the cutoff frequency of the continuum radiation, the plasma frequency, and the upper hybrid resonance frequency. Burst mode data sampling (up to 35 k samples/s) is included for time domain analysis of whistler and other waves. The Japanese Exploration of energization and Radiation in Geospace (ERG) spacecraft, planned for launch in 2015, will have a similar instrumentation with the important addition of the Software-Wave Particle Interaction Analyzer (S-WPIA), which determines $\mathbf{v} \cdot \mathbf{E}$ (= rate of particle energization) at the time scale of the whistler wave period (Fukuhara et al. 2009, Miyoshi et al. 2012).

It is necessary to combine other experimental resources to obtain a more global view of the inner magnetosphere and address ionospheric effects on magnetospheric phenomena. Experiments commonly used in conjunction with equatorial satellites include the following: low earth orbit (LEO) satellites (e.g., Kohnert et al. 2011); balloons (e.g., Millan et al. 2013); radars (e.g., Baker et al. 2010); magnetometers (e.g., Ozeke et al. 2012); LF-radio standard networks (Clilverd et al. 2009); and GPS receivers (e.g., Foster and Erickson 2013).

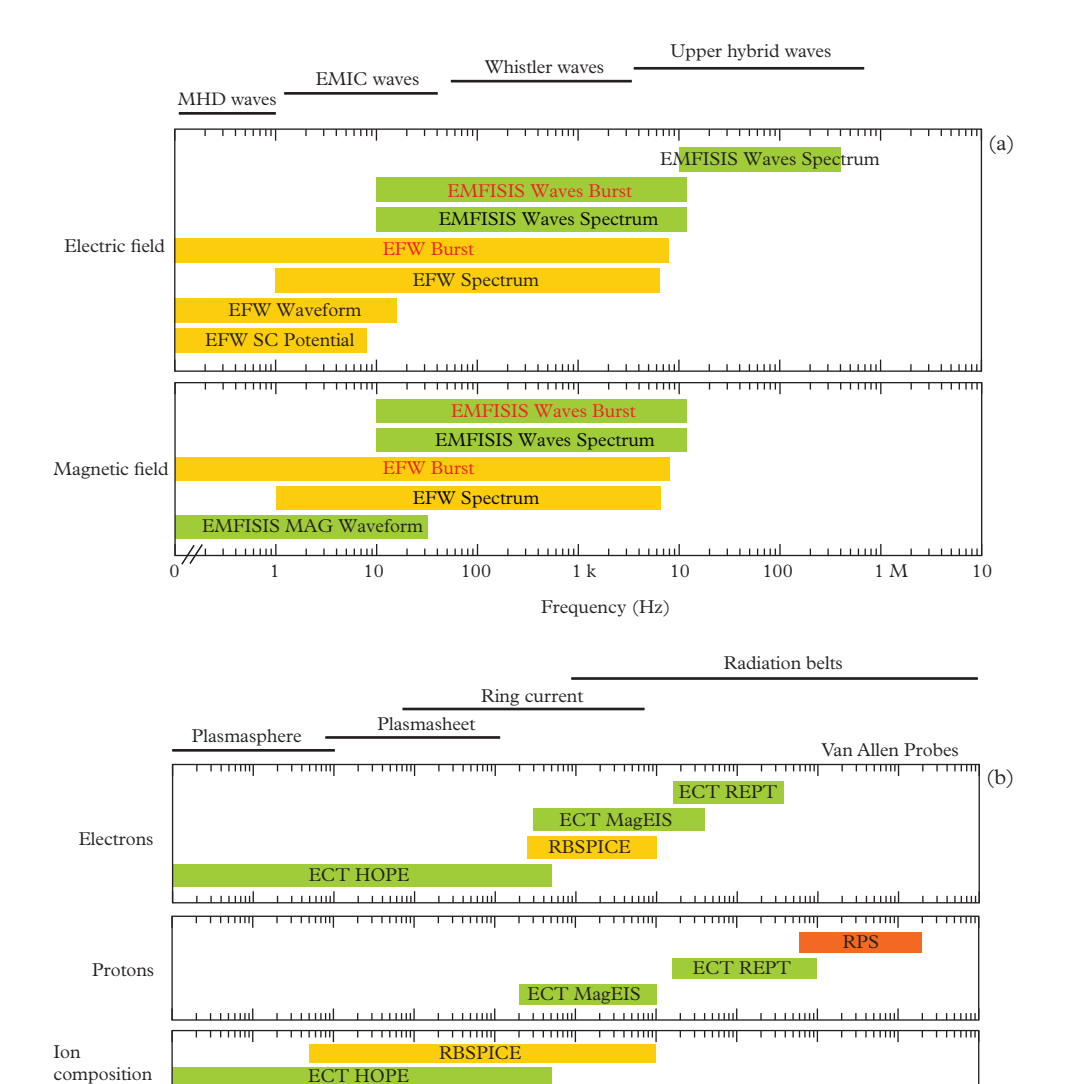


Figure 2.3 Van Allen Probes experiment capabilities and their relations to waves and particles.
(a) Field experiments. Typical frequency bands occupied by different wave modes are shown at the top. (b) Particle experiments. Typical energy ranges of particles in different magnetospheric regions are shown at the top.

100

Energy (eV)

10

10

100

1G

1M

1k

100

10

2.5 Example of observational studies of waves and particles

This section presents examples of studies of wave-particle interactions in the inner magnetosphere.

2.5.1 ULF wave-particle interaction

The duty cycle (one energy sweep) of a particle detector is typically shorter than the period of Pc4-5 waves (45–600 s). Therefore, ULF waves are unique in that we can detect the signatures of particle resonances in time series data. In the adiabatic approximation (magnetic moment is conserved), the modulation of the flux, δF , of particles executing drift motion in a wave with an azimuthal electric field δE_{φ} is expressed as (e.g., Southwood 1976)

$$\delta F \propto \frac{i\delta E_{\varphi}}{(\omega - m\omega_{\rm d} - N\omega_{\rm b})} e^{-i(\omega t - m\varphi)}$$
 (2.1)

where ω and m are the frequency and azimuthal wavenumber of the wave, ω_d and ω_b are the drift and bounce frequencies of the particles, and N is an integer. This equation predicts that the amplitude of δF peaks at the particle energy corresponding to the resonance

$$\omega - m\omega_{\rm d} - N\omega_{\rm b} = 0 \tag{2.2}$$

and that the phase of δF relative to δE_{φ} changes by 180° across the resonance energy.

Figure 2.4 shows in-situ observation of a ULF wave-particle resonance phenomenon (Dai et al. 2013). In this example, Van Allen Probe-A detected an azimuthally polarized 84-s (Pc4) oscillation in the electric field (Figure 2.4a) not too far from the magnetic equator. The electric field oscillation is accompanied by a radially polarized magnetic field oscillation (Figure 2.4b). By comparing the observed wave period and the δE_{φ} - δB_r relationship with a theoretical model, it was concluded that the oscillations had a fundamental standing Alfvén wave structure along the ambient magnetic field. This structure requires N to be an even number (Southwood and Kivelson 1982), meaning that the drift resonance $\omega - m\omega_{\rm d} = 0$ (a special case of N=0 in Equation 2.2) is possible.

The theoretically expected particle behavior is evident. First, the fluxes of ions (assumed to be protons) measured at 7 energy steps between 60 keV and 170 keV all oscillate with the same period as the wave (Figure 2.4c). Second, the amplitude of the flux oscillation is energy dependent, with the maximum amplitude occurring at \sim 90 keV. Finally, there is a shift of the oscillation phase with energy. The cross phase relative to δE_{φ} increases with energy, with the zero crossing occurring at \sim 90 keV.

Drift resonance with protons requires the wave to be propagating in the same direction as the proton guiding center drift. This immediately tells us that the wave was

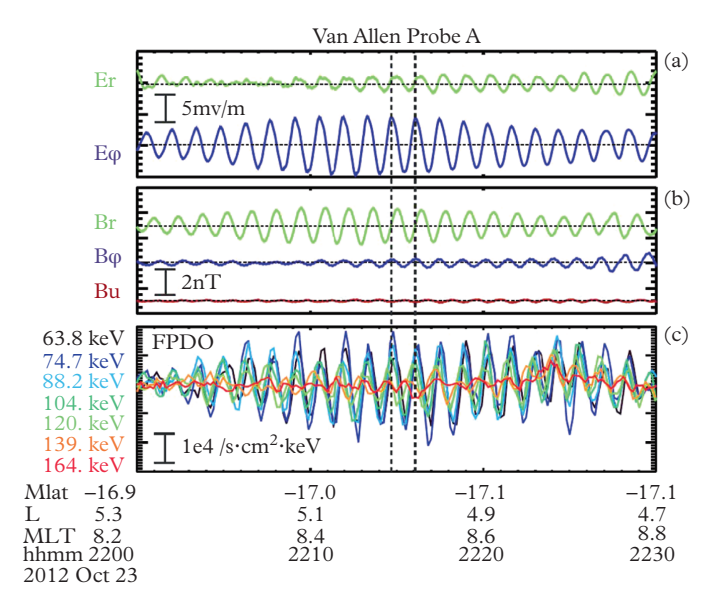


Figure 2.4 Observation of ion drift resonance with Van Allen Probe-A (Dai et al. 2013). (a) The radial (r) and azimuthal (φ) components of the electric field during a monochromatic 84-s (Pc4) ULF wave event. Two vertical dashed lines are drawn through the peaks of the E_{φ} component. (b) The three components of the magnetic field. The B_{μ} component is along the average magnetic field. (c) Omnidirectional ion (assumed to be protons) flux measured in 7 energy channels.

propagating westward. Furthermore, with the measured wave frequency and the known dependence of ω_d on particle energy, the azimuthal wave number is found to be -70. The large magnitude of m is consistent with the wave being a poloidal mode (radial oscillations of field lines) and points to an internal instability. In fact, the examination of the ion phase space density indicated an inward gradient that can destabilize a fundamental poloidal wave through drift resonance (Southwood 1976, Chen and Hasegawa 1988).

2.5.2 Two-spacecraft measurements of wave propagation

We need to know both the frequency and wave vector to determine how waves interact with particles. With a single spacecraft we can measure the frequency but not the wavenumber unless there is a clear particle resonance signature as seen in Figure 2.4. Observational determination of wavelengths or wavenumbers is a major challenge, for example, in evaluating the effectiveness of electron radial diffusion by ULF waves (e.g., Tu et al. 2012). When we have multiple spacecraft, it is possible to determine the wavenumber using phase delay analysis.

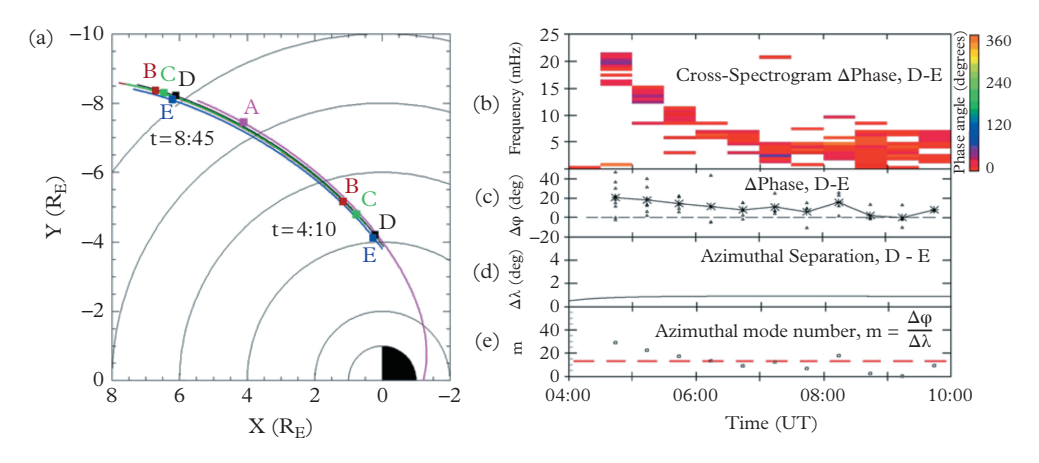


Figure 2.5 Wavenumber analysis for ULF waves using THEMIS spacecraft (Sarris et al. 2009).
(a) Location of the THEMIS probes on 4 September 2007 in the X-Y plane of the geocentric solar ecliptic coordinate system. The dots indicate the locations at 0410 UT and 0845 UT. (b) Cross phase between the radial components of the electric field measured by THEMIS-D and THEMIS-E, plotted as a function of time and frequency. A color key is used to indicate the cross phase value. (c) Phase difference between the two probes. (d) Azimuthal separation of the two probes. (e) Azimuthal wave number.

Figure 2.5 illustrates an example of phase delay analysis applied to ULF waves observed from THEMIS-D and -E (Sarris et al. 2009). The frequency of the waves decreased with L (Figure 2.5b) as expected for standing Alfvén waves excited on local field lines. From comparison of the radial electric field and the azimuthal magnetic field components, it was concluded that the oscillations were fundamental toroidal waves (azimuthal oscillations of field lines). The spacecraft maintained a small azimuthal separation (Figure 2.5d) as they moved from L=4 (0400 UT) to L=12 (1000 UT). The small separation eliminates the $2n\pi$ ambiguity in cross phase. The toroidal waves observed by the two spacecraft had high coherence, and it was possible to determine the phase delay continuously (Figure 2.5c). The m number derived from the phase delay is mostly near 15, which is substantially smaller than that of the fundamental poloidal wave shown in Figure 2.4. Low m values are expected for waves driven by the solar wind.

2.5.3 Ground-satellite observation of EMIC waves, aurora, and particle precipitation

With the above two examples, we described how spacecraft measurements in the equatorial magnetosphere are used to study wave properties and wave-particle interactions. However, the consequence of the local wave-particle interaction on global particle population is difficult to address unless we make additional measurements. The question is whether waves cause a sufficient amount of particle transport to produce

large changes in the particle flux in the radiation belt and ring current. For example, are a large number of particles lost through wave-particle interactions? For loss mechanisms involving particle precipitation into the atmosphere, ground-based observation and low-altitude satellite or balloon observations provide valuable information.

Figure 2.6 shows the result of a study (Miyoshi et al. 2008) taking the above approach. In this example, a search coil magnetometer on the ground detected EMIC waves while an all-sky camera took 2d images of emissions caused by precipitating ions (tens of keV). The EMIC waves occurred in the helium band, and the all-sky camera detected localized proton aurora, which were taken as evidence that the EMIC waves

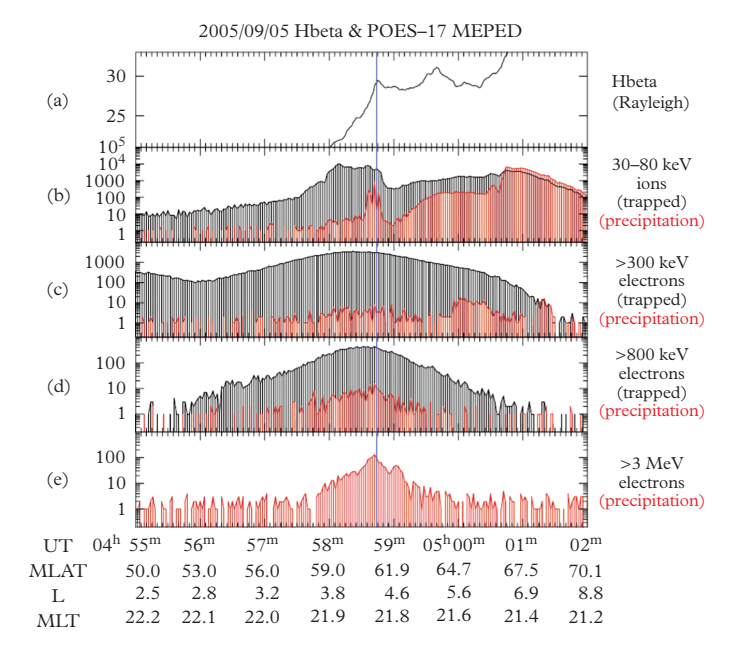


Figure 2.6 Observation of particle precipitation associated with EMIC waves observed on the ground (Miyoshi et al. 2008).

(a) Emission at the Hydrogen Balmer line captured by an all-sky camera and averaged over 0430–0500 UT on September 5, 2005. The field of view of the camera covered the magnetic field footpoint of the POES-17 satellite for 0455–0502 UT, and the plot shows the time-averaged emission intensity evaluated along the footpoint over this time interval. The location of the satellite is shown at the bottom of the figure using magnetic latitude (MLAT), magnetic shell L value, and magnetic local time (MLT). The vertical blue line indicates the time when the satellite footprint crossed the stable isolated proton aurora. (b–e) Intensity of the flux (detector count rate) of electrons and ions measured by the POES-17 satellite, plotted as a function of universal time. Trapped and precipitating particles are shown in black and light grey, respectively.

pitch angle scattered the protons into the loss cone. Making this event even more unique, the low-altitude satellite POES-17 traversed the field of view of the all-sky camera. The particle instruments on this satellite detected simultaneously occurring peaks in the flux of precipitating ions (30–80 keV, Figure 2.6b) and precipitating relativistic electrons (>3 MeV, Figure 2.6e), which spatially matched an intensity peak of the proton aurora (Figure 2.6a). These observations led Miyoshi et al. to conclude that the EMIC waves caused precipitation of both ions and electrons. This type of wave-particle interaction was predicted theoretically (Cornwall et al. 1970; Thorne and Kennel 1971).

2.5.4 Nonlinear wave-particle interactions

Until now, linear and quasilinear theories have mainly been employed to describe wave-particle interactions in the inner magnetosphere. However, nonlinear processes could play a major role, and future experimental studies need to address them. To emphasize this point, we consider recent theoretical studies and computer simulation of nonlinear wave-particle interactions associated with whistler (chorus) and EMIC waves. First, the so-called nonlinear trapping process produces electromagnetic electron and ion holes in the velocity phase space, which respectively generate whistler and EMIC waves through the resonant current (Omura et al. 2010, 2012). Second, computer simulations produced triggered whistler and EMIC emissions with rising tones (e.g., Hikishima et al. 2009, Shoji and Omura 2013), which are very similar to real observations (Santolik et al. 2003, Sakaguchi et al. 2013). Third, a THEMIS study confirmed that the observed variations of chorus amplitude are consistent with the nonlinear theory (Kurita et al. 2012). Finally, nonlinear processes lead to strong electron accelerations by chorus waves and rapid precipitation of electrons by EMIC waves (Katoh et al. 2008, Omura and Zhao 2013).

To understand the details of nonlinear wave-particle interactions, it is necessary to conduct time domain measurements of both wave fields and particle fluxes. Specifically, the measurements need to be made with a time resolution higher than the period of relevant waves. The fields experiments on the Van Allen Probes are capable of making the required fields measurements in the EMIC and whistler bands, but particle fluxes are not measured in high enough time resolution. Therefore, it is expected that the S-WPIA experiment on the ERG spacecraft (see Section 2.4) will shed a new light on the nonlinear processes involving whistler waves.

2.6 Summary

In summary, we have presented examples of observational studies of wave-particle interactions in the magnetosphere. The purpose was to provide information on the experimental resources available to us and how these resources can be used. Important factors in experimental studies are the orbits of spacecraft and instrumentation. We reviewed studies of wave-particle interactions involving ULF, EMIC, and VLF waves. The focus was on how to take advantage of multi-instrument observation and

simultaneous observations from multiple spacecraft. We also emphasized the importance of additional experimental resources to address the global consequence of wave-particle interactions.

Acknowledgments

Work at JHU/APL was supported by NASA grants NNX10AK93G and NNX14AB97G and by the Van Allen Probes mission. Work at the Solar-Terrestrial Environment Laboratory at Nagoya University was supported by Grants-in-Aid for Scientific Research (23340146, 23224011) of the Japan Society for the Promotion of Science.

.....

REFERENCES

- Angelopoulos, V. (2008). The THEMIS Mission. *Space Sci. Rev.*, **141**, 5–34, doi:10.1007/s11214-008-9336-1.
- Baker, D. N., et al. (2013). The Relativistic Electron-Proton Telescope (REPT) instrument on board the Radiation Belt Storm Probes (RBSP) spacecraft: Characterization of Earths radiation belt high-energy particle populations. *Space Sci. Rev.*, 179, 337–381, doi:10.1007/s11214-012-9950-9.
- Baker, J. B. H., et al. (2010). Monitoring ionospheric space weather with the Super Dual Auroral Radar Network (SuperDARN). Radar Conference, 2010 IEEE, 1414–1417, doi:10.1109/RADAR.2010.5494396.
- Blake, J. B., et al. (2013). The Magnetic Electron Ion Spectrometer (MagEIS) instruments aboard the Radiation Belt Storm Probes (RBSP) spacecraft. *Space Sci. Rev.*, **179**, 383–421, doi:10.1007/s11214-013-9991-8.
- Bortnik, J., and R. M. Thorne (2010). Transit time scattering of energetic electrons due to equatorially confined magnetosonic waves. *J. Geophys. Res.*, 101(A1), 479–493, doi:10.1029/95JA02985.
- Chen, L., and A. Hasegawa (1988), On magnetospheric hydromagnetic waves excited by energetic ring-current particles. J. Geophys. Res., 93(A8), 8763–8767, doi:10.1029/JA093iA08p08763.
- Claudepierre, S. G., S. R. Elkington, and M. Wiltberger (2008). Solar wind driving of magnetospheric ULF waves: Pulsations driven by velocity shear at the magnetopause. *J. Geophys. Res.*, 113, A05218, doi:10.1029/2007JA012890.
- Clilverd, M. A., et al. (2009), Remote sensing space weather events: Antarctic-Arctic Radiation-belt (Dynamic) Deposition-VLF Atmospheric Research Konsortium network. *Space Weather*, 7, S04001, doi:10.1029/2008SW000412.
- Cornwall, J. M., F. V. Coroniti, and R. M. Thorne (1970), Turbulent loss of ring current protons. *J. Geophys. Res.*, 75(25), 4699–4709.
- Dai, L., et al. (2013). Excitation of poloidal standing Alfvén waves through drift resonance waveparticle interaction. *Geophys. Res. Lett.*, **40**, 4127–4132, doi:10.1002/grl.50800.
- Elkington, S. R., M. K. Hudson, and A. A. Chan (1999). Acceleration of relativistic electrons via drift-resonant interaction with toroidal-mode Pc-5 ULF oscillations. *Geophys. Res. Lett.*, 26(21), 3273–3276.

- Fälthammar, C. G. (1965). Effects of time-dependent electric fields on geomagnetically trapped radiation. J. Geophys. Res., 70(11), 2503–2516.
- Foster, J. C., and P. J. Erickson (2013). Ionospheric superstorms: Polarization terminatoreffects in the Atlantic sector. *J. Atmos. Solar-Terr. Phys.*, **103**, 147–156, doi:10.1016/j.jastp.2013.04.001.
- Frey, S., V. Angelopoulos, M. Bester, J. Bonnell, T. Phan, and D. Rummel (2008). Orbit Design for the THEMIS Mission. *Space Sci. Rev.*, 141, 61–89, doi:10.1007/s11214-008-9441-1.
- Fukuhara, H., H. Kojima, Y. Ueda, Y. Omura, Y. Katoh, and H. Yamakawa (2009). A new instrument for the study of wave-particle interactions in space: One-chip Wave-Particle Interaction Analyzer. *Earth Planets Space*, **61**, 765–778.
- Funsten, H. O., et al. (2013). Helium, Oxygen, Proton, and Electron (HOPE) Mass Spectrometer for the Radiation Belt Storm Probes Mission. *Space Sci. Rev.*, **179**, 423–484, doi:10.1007/s11214-013-9968-7.
- Hamilton, D. C., G. Gloeckler, and F. M. Ipavich (1988). Ring current development during the great geomagnetic storm of February 1986. *J. Geophys. Res.*, 93(A12), 14343–14355.
- Hikishima, M., S. Yagitani, Y. Omura, and I. Nagano (2009). Full particle simulation of whistler-mode rising chorus emissions in the magnetosphere. J. Geophys. Res., 114, A01203, doi:10.1029/2008JA013625.
- Horne, R. B., R. M. Thorne, S. A. Glauert, N. P. Meredith, D. Pokhotelov, and O. Santolík (2007), Electron acceleration in the Van Allen radiation belts by fast magnetosonic waves. *Goephys. Res. Lett.*, 34, L17107, doi:10.1029/2007GL030267.
- Hudson, M. K., B. T. Kress, H.-R. Mueller, J. A. Zastrow, and J. B. Blake (2008). Relationship of the Van Allen radiation belts to solar wind drivers. *J. Atmos. Solar-Terr. Phys.*, 70(5), 708–729.
- Katoh, Y., Y. Omura, and D. Summers (2008). Rapid energization of radiation belt electrons by nonlinear wave trapping. *Ann. Geophys.*, 26, 3451–3456, doi:10.5194/angeo-26-3451-2008.
- Kennel, C. F., and H. E. Petschek (1966). Limit on stably trapped particle fluxes. J. Geophys. Res., 71, 1.
- Kletzing, C. A., et al. (2013). The Electric and Magnetic Field Instrument Suite and Integrated Science (EMFISIS) on RBSP. *Space Sci. Rev.*, doi:10.1007/s11214-013-9993-6.
- Kohnert, R., S. Palo, and X. Li (2011). Small space weather research mission designed fully by students. *Space Weather*, **9**(4), doi:10.1029/2011SW000668.
- Kurita, S., Y. Katoh, Y. Omura, V. Angelopoulos, C. M. Cully, O. Le Contel, and H. Misawa (2012). THEMIS observation of chorus elements without a gap at half the gyrofrequency. *J. Geophys. Res.*, 117, A11223, doi:10.1029/2012JA018076.
- Li, X., D. N. Baker, T. P. O'Brien, L. Xie, and Q. G. Zong (2006). Correlation between the inner edge of outer radiation belt electrons and the innermost plasmapause location. *Geophys. Res. Lett.*, 33, L14107, doi:10.1029/2006GL026294.
- Mauk, B. H., N. J. Fox, S. G. Kanekal, R. L. Kessel, D. G. Sibeck, and A. Ukhorskiy (2013). Science Objectives and rationale for the Radiation Belt Storm Probes Mission. *Space Sci. Rev.*, 179, 3–27, doi:10.1007/s11214-012-9908-y.
- Mazur, J., et al. (2013). The Relativistic Proton Spectrometer (RPS) for the Radiation Belt Storm Probes Mission. *Space Sci. Rev.*, 179, 221–261, doi:10.1007/s11214-012-9926-9.
- Meredith, N. P., R. B. Horne, and R. R. Anderson (2008). Survey of magnetosonic waves and proton ring distributions in the Earth's inner magnetosphere. *J. Geophys. Res.*, 113, A06213, doi:10.1029/2007JA012975.
- Meredith, N. P., R. B. Horne, R. H. A. Iles, R. M. Thorne, D. Heynderickx, and R. R. Anderson (2002). Outer zone relativistic electron acceleration associated with substorm-enhanced whist-ler mode chorus. *J. Geophys. Res.*, 107(A7), 1144, doi:10.1029/2001JA900146.

- Millan, R. M., et al. (2013). The Balloon Array for RBSP Relativistic Electron Losses (BARREL). Space Sci. Rev., 179, 503–530, doi:10.1007/s11214-013-9971-z.
- Mitchell, D. G., et al. (2013). Radiation Belt Storm Probes Ion Composition Experiment (RBSPICE). Space Sci. Rev., 179, 263–308, doi:10.1007/s11214-013-9965-x.
- Miyoshi, Y., et al. (2012). The Energization and Radiation in Geospace (ERG) project, in *Dynamics of the Earth's Radiation Belts and Inner Magnetosphere*, vol. 119, edited by D. Summers et al., AGU, Washington, D. C.
- Miyoshi, Y., K. Sakaguchi, K. Shiokawa, D. Evans, J. Albert, M. Connors, and V. Jordanova (2008). Precipitation of radiation belt electrons by EMIC waves, observed from ground and space. *Geophys. Res. Lett.*, 35, L23101, doi:10.1029/2008GL035727.
- Miyoshi, Y., R. Kataoka, Y. Kasahara, A. Kumamoto, T. Nagai, and M. F. Thomsen (2013). High-speed solar wind with southward interplanetary magnetic field causes relativistic electron flux enhancement of the outer radiation belt via enhanced condition of whistler waves. *Geophys. Res. Lett.*, 40, 4520–4525.
- Omura, Y., D. Nunn, and D. Summers (2012). Generation processes of whistler mode chorus emissions: Current status of nonlinear wave growth theory, in *Dynamics of the Earth's Radiation Belts and Inner Magnetosphere*, *Geophys. Monogr. Ser.*, vol. 199, edited by D. Summers et al., pp. 243–254, AGU, Washington, D. C., doi:10.1029/2012GM001347.
- Omura, Y., J. Pickett, B. Grison, O. Santolík, I. Dandouras, M. Engebretson, P. M. E. Dcrau, and A. Masson (2010). Theory and observation of electromagnetic ion cyclotron triggered emissions in the magnetosphere. *J. Geophys. Res.*, 115, A07234, doi:10.1029/2010JA015300.
- Omura, Y., and Q. Zhao (2013). Relativistic electron microbursts due to nonlinear pitch angle scattering by EMIC triggered emissions. *J. Geophys. Res.*, 118, 5008–5020, doi:10.1002/jgra.50477.
- Ozeke, L. G., and I. R. Mann (2001). Modeling the properties of high-*m* Alfvén waves driven by the drift-bounce resonance mechanism. *J. Geophys. Res.*, **106**, 15583–15597.
- Ozeke, L. G., I. R. Mann, K. R. Murphy, I. J. Rae, D. K. Milling, S. R. Elkington, A. A. Chan, and H. J. Singer (2012). ULF wave derived radiation belt radial diffusion coefficients. *J. Geophys. Res.*, 117, A04222, doi:10.1029/2011JA017463.
- Reeves, G. D., K. L. McAdams, R. H. W. Friedel, and T. P. O'Brien (2003). Acceleration and loss of relativistic electrons during geomagnetic storms. *Geophys. Res. Lett.*, 30(10), 1529, doi:10.1029/2002GL016513.
- Russell, C. T., R. E. Holzer, and E. J. Smith (1970). OGO 3 observations of ELF noise in the magnetosphere: 2. The nature of the equatorial noise. *J. Geophys. Res.*, 75(4), 755–768, doi:10.1029/JA075i004p00755.
- Sakaguchi, K., Y. Kasahara, M. Shoji, Y. Omura, Y. Miyoshi, T. Nagatsuma, A. Kumamoto, and A. Matsuoka (2013). Akebono observations of EMIC waves in the slot region of the radiation belts. *Geophys. Res. Lett.*, 40, 1–5, doi:10.1002/2013GL058258.
- Santolík, O., D. A. Gurnett, J. S. Pickett, M. Parrot, and N. Cornilleau-Wehrlin (2003). Spatio-temporal structure of storm-time chorus. J. Geophys. Res., 108, 1278, doi:10.1029/2002JA009791.
- Sarris, T. E., W. Liu, K. Kabin, X. Li, S. R. Elkington, R. Ergun, R. Rankin, V. Angelopoulos, J. Bonnell, K. H. Glassmeier, and U. Auster (2009), Characterization of ULF pulsations by THEMIS. *Geophys. Res. Lett.*, 36, L04104, doi:10.1029/2008GL036732, 2009.
- Schulz, M., and L. Lanzerotti (1974). Particle Diffusion in the Radiation Belts. Springer, Berlin.
- Shoji, M., and Y. Omura (2013). Triggering process of electromagnetic ion cyclotron rising tone emissions in the inner magnetosphere. *J. Geophys. Res.*, 118, 5553–5561, doi:10.1002/jgra.50523.

- Shprits, Y. Y., D. A. Subbotin, N. P. Meredith, and S. R. Elkington (2008b). Review of modeling of losses and sources of relativistic electrons in the outer radiation belt II: Localacceleration and loss. *J. Atmos. Solar-Terr. Phys.*, 70, 1694–1713.
- Shprits, Y. Y., S. R. Elkington, N. P. Meredith, and D. A. Subbotin (2008a). Review of modeling of losses ands ources of relativistic electrons in the outer radiation belt I: Radial transport. J. Atmos. Solar-Terr. Phys., 70, 1679–1693.
- Singer, H. J., L. Matheson, R. Grubb, A. Newman, and S. D. Bouwer (1996). Monitoring space weather with the GOES magnetometers. *Proc. SPIE Int. Soc. Opt. Eng.* 2812, 299–308.
- Southwood, D. J. (1976). A general approach to low-frequency instability in the ring current plasma. J. Geophys. Res., 81(19), 3340–3348.
- Southwood, D. J., and M. G. Kivelson (1982). Charged particle behavior in low-frequency geomagnetic pulsations, 2, Graphical approach. J. Geophys. Res., 87(A3), 1707–1710.
- Summers, D., C. Ma, N. P. Meredith, R. B. Horne, R. M. Thorne, D. Heynderickx, and R. R. Anderson (2002). Model of the energization of outer-zone electrons by whistler-mode chorus during the October 9, 1990 geomagnetic storm. *Geophys. Res. Lett.*, 29(24), 2174, doi:10.1029/2002GL016039.
- Thorne, R. M. (2010). Radiation belt dynamics: The importance of wave-particle interactions. *Geophys. Res. Lett.*, 37, L22107, doi:10.1029/2010GL044990.
- Thorne, R. M., and C. F. Kennel (1971). Relativistic electron precipitation during magnetic storm main phase. *J. Geophys. Res.*, 76(19), 4446–4453.
- Tsurutani, B. T., and E. J. Smith (1974). Postmidnight chorus: A substorm phenomenon. *J. Geophys. Res.*, 79(1), 118–127.
- Tu, W., S. R. Elkington, X. Li, W. Liu, and J. Bonnell (2012). Quantifying radial diffusion coefficients of radiation belt electrons based on global MHD simulation and spacecraft measurements. J. Geophys. Res., 117, A10210.
- Turner, D. L., V. Angelopoulos, W. Li, M. D. Hartinger, M. Usanova, I. R. Mann, J. Bortnik, and Y. Shprits (2013). On the storm-time evolution of relativistic electron phase space density in Earth's outer radiation belt. J. Geophyts. Res., 118(5), 2196–2212, doi:10.1002/jgra.50151.
- Ukhorskiy, A. Y., and M. I. Sitnov (2012). Dynamics of Radiation Belt Particles. *Space Sci. Rev.*, doi:10.1007/s11214-012-9938-5.
- Ukhorskiy, A. Y., Y. Y. Shprits, B. J. Anderson, K. Takahashi, and R. M. Thorne (2010). Rapid scattering of radiation belt electrons by storm-time EMIC waves. *Geophys. Res. Lett.*, 37, L09101, doi:10.1029/2010GL042906.
- Wygant, J. R., et al. (2013). The Electric Field and Waves Instruments on the Radiation Belt Storm Probes Mission. *Space Sci. Rev.*, 179, 183–220, doi:10.1007/s11214-013-0013-7.